

# The Reconstruction Software for the MICE Scintillating Fibre Trackers

A. Dobbs, C. Hunt, K. Long, E. Santos

*Physics Department, Blackett Laboratory, Imperial College London*

*Exhibition Road, London, SW7 2AZ, UK*

P. Kyberd

*Brunel University London, Kingston Lane, Uxbridge, Middlesex, UB8 3PH, U.K.*

C. Heidt

*University of California Riverside, 900 University Ave, Riverside, CA 92521, U.S.A.*

A report on the reconstruction software of the scintillating fibre trackers of the Muon Ionization Cooling Experiment (MICE). MICE will demonstrate the principle of muon beam emittance reduction via ionisation cooling for the first time, for application in future muon accelerator-based facilities, such as a Neutrino Factory or Muon Collider. The beam emittance before and after cooling is required to be measured to high precision, which is to be achieved with two scintillating fibre trackers, one upstream and one downstream of the cooling channel. This paper describes the reconstruction software of the fibre trackers, including the GEANT4 based simulation, geometry and configuration implementations, digitisation, spacepoint reconstruction, pattern recognition and the final track fit based on a Kalman filter. The performance of the software is evaluated by means of MC studies using momentum residuals and various other methods, and the precision of the final track parameter reconstruction evaluated.

## 1 The MICE Experiment

### 1.1 Overview

The Muon Ionization Cooling Experiment (MICE) will be the first practical demonstration of ionization cooling of muons. Cooling refers to a reduction in the emittance of a beam, that is, the phase space volume occupied. Beam cooling is required for any future facility based on high intensity muon beams, such as a Neutrino Factory [1], the ultimate tool to study leptonic CP symmetry violation, or Muon Collider [2], a potential route to multi-TeV lepton - anti-lepton collisions. Muon beams are generated via pion decay, leading to a large initial phase space distribution, which must be shrunk in order for a reasonable fraction of the beam to fall within the acceptance of downstream acceleration components. Without cooling much of the muon beam is lost, leading to a severe reduction in useful particle rates.

The short muon lifetime requires a fast beam cooling technique which traditional cooling techniques are unable to provide. Ionisation cooling was proposed in the early 1970s [3, 4], but has yet to be demonstrated. Ionization cooling reduces beam emittance by first passing a beam through some suitable, low atomic number material, such as a hydrogen. This leads to reduction in beam momentum in all directions due to ionisation energy losses. After the absorber, momentum is restored in the longitudinal direction only by means of RF cavities. The sequence is repeated leading to an overall reduction in the transverse phase space of the beam.

MICE will represent the first practical demonstration of muon cooling. A schematic of the full MICE cooling channel, including ionisation energy loss and longitudinal acceleration, is shown in figure 1.

MICE is based at Rutherford Appleton Laboratory, U.K., using the ISIS synchrotron as a proton driver to generate the muon beam. The MICE beamline is described in detail in [5]. MICE recently completed

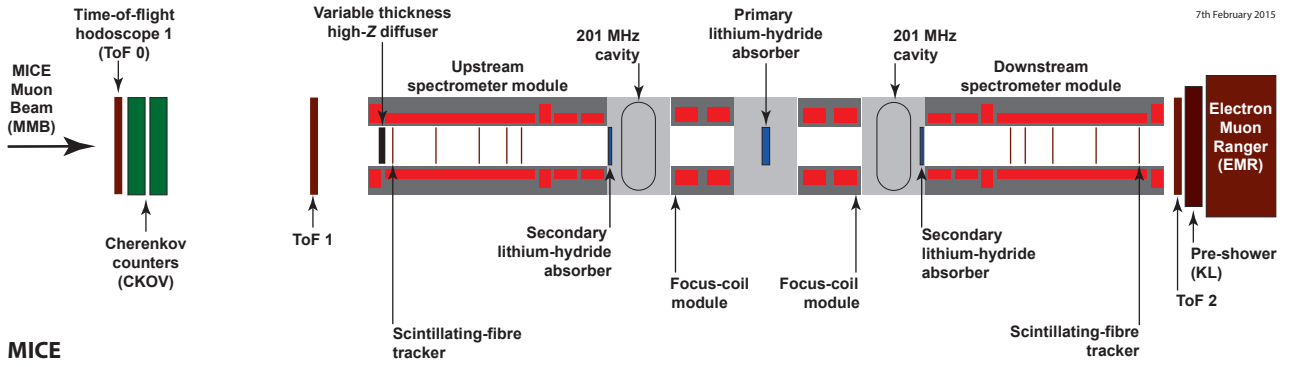


Figure 1: The downstream beam line and final cooling channel. The diffuser is used to increase the beam emittance prior to cooling. The primary absorber can be swapped between liquid hydrogen and solid lithium hydride.

Step I of its programme, consisting of the muon beamline with particle identification (PID). The next step in the programme, Step IV, which introduced the trackers and the first absorber module, producing transverse emittance reduction, began taking data in 2015. The demonstration of sustainable cooling, which includes longitudinal re-acceleration, will begin data taking in 2018.

## 1.2 The Scintillating Fibre Trackers

MICE is equipped with two identical, high precision scintillating fibre (“scifi”) trackers, described in [6]. Each tracker is housed in a superconducting solenoid that provides a uniform 4 T field over the tracking volume. Tracker 1 is located upstream of the cooling channel, Tracker 2 downstream. Each tracker consists of 5 detector stations, labelled 1 to 5, as illustrated in figure 2. The upstream tracker, TKU, is orientated such that Station 5 sees the beam first, while the downstream tracker, TKD, is rotated by  $180^\circ$  such that Station 1 sees the beam first, thus in both trackers Station 1 is always nearest to the cooling channel (see figure 1).

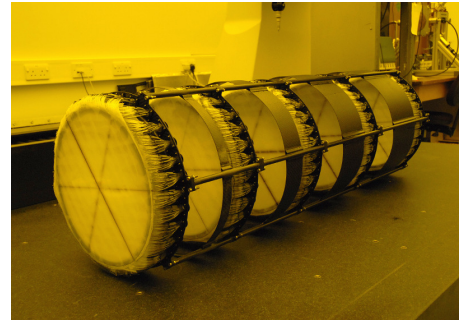
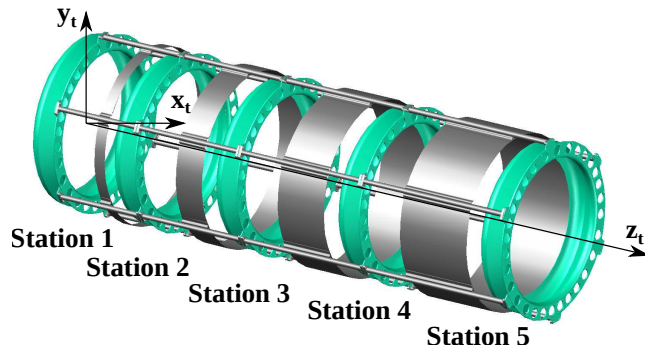


Figure 2: Left: A schematic of the tracker carbon fibre frame, showing the detector station positions. The fibre planes are glued on to the upstream edge (smaller  $z_t$  position) of the carbon fibre station frames (shown in green). Right: A photograph of a tracker. The orange tint is due to the special lighting needed to protect the fibres. The intersecting lines visible on the station faces indicates the direction of the fibres in each plane.

Each station is formed of three planes of  $350 \mu\text{m}$  scintillating fibres, orientated at 120 degrees to each other, attached to a sheet of mylar plastic. The fibres in each plane are arranged in a doublet-layer structure in order to give 100% coverage of the plane area as illustrated in figure 3. A mylar sheet glued to the doublet layer

provides mechanical stability. The fibres are collected into groups of seven for readout, each group forming a single channel, as illustrated in figure 3b. The planes, also known as views, are labelled  $U$ ,  $V$  and  $W$ . Plane  $U$  is attached to the station frame directly, plane  $W$  on to plane  $U$ , and plane  $V$  on to plane  $W$ . The fibre plane orientations are illustrated in figure 4. Each station is oriented such that the fibres in the  $U$  plane are vertical. The fibres produce scintillation light when ionising radiation passes through them. Clear-fibre light guides transport the scintillation light to visible light photon counters (VLPCs) in a cryostat for readout (see [6] for details).

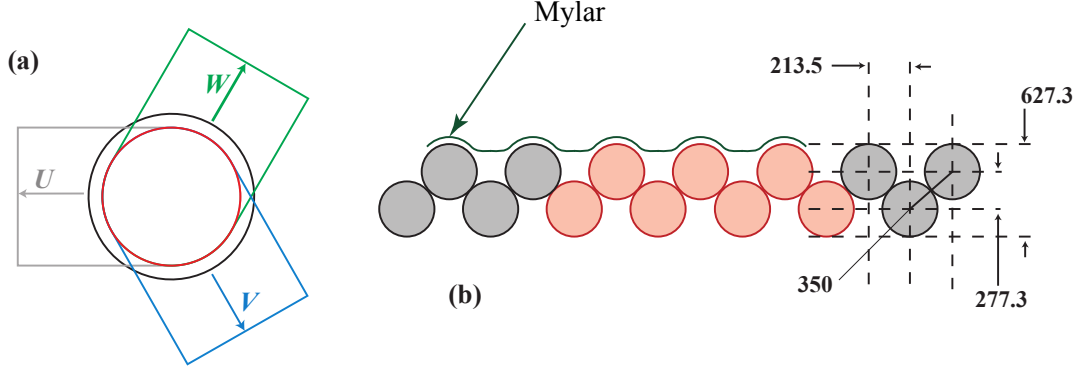


Figure 3: (a) Arrangement of the doublet layers in the scintillating-fibre stations. The outer circle shows the solenoid bore while the inner circle shows the limit of the active area of the tracker. The arrows indicate the direction that the individual  $350\ \mu\text{m}$  fibres run. (b) Detail of the arrangement of the scintillating fibres in a doublet layer. The fibre spacing and the fibre pitch are indicated on the right-hand end of the figure in  $\mu\text{m}$ . The pattern of seven fibres ganged for readout as a single channel, via a single clear-fibre light-guide, is shown in red. The sheet of mylar plastic glued to the doublet layer is indicated.

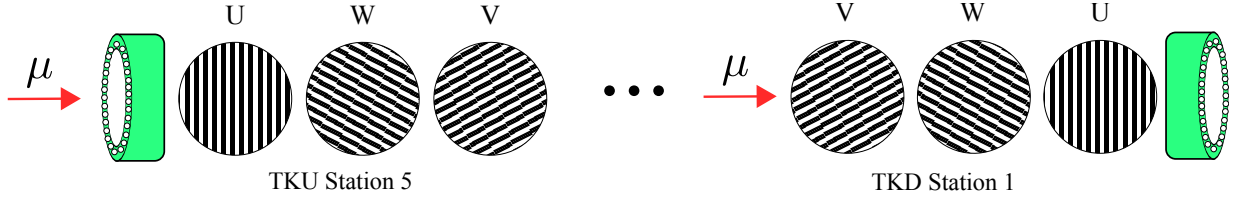


Figure 4: The orientation of the fibres in each plane, as seen by the incoming beam, for both trackers. The green object is station frame. If TKU was rotated by  $180^\circ$  around the centre of the cooling channel, it would be coincident TKD.

## 2 Coordinate systems and Reference Surfaces

### 2.1 Channels and Digits

The  $V$  and  $W$  planes each consist of 214 channels, labelled 0 to 213, while the  $U$  plane has 212 channels, labelled 0 to 211. The channel number increases from left to right if a plane is placed mylar side up, with the fibre readout pointing downwards, as illustrated in figure 5.

## 70 2.2 Planes and Clusters

The plane reference surface is defined to be the flat plane that is formed by the outer surface of the mylar sheet. The measured position perpendicular to the direction of the fibres in each plane is labelled  $\alpha \in (v, u, w)$ , defined to increase in the *opposite* direction to the channel number.  $\alpha$  is then given by:

$$\alpha = (N_{CC} - N_{Ch}) \times p \times d \quad (1)$$

75 where  $N_{CC}$  is the central channel number,  $N_{Ch}$  is the channel number,  $p$  is the channel pitch, that is twice the horizontal distance between neighbouring fibres ( $2 \times 213.5 = 417$  mm) , and  $d$  is half the number of fibres in a channel, i.e. 3.5 (see figure 3, it can be seen  $p \times d$  is just the width of a channel).

The  $z$  axis of the plane coordinate system is defined to be perpendicular to the plane reference surface and points in the direction from the mylar sheet towards the fibres. The direction in which the fibres run defines the final plane coordinate,  $\beta$ , with the direction defined to complete a right-handed coordinate system. The origin  
80 of the  $(\alpha, \beta)$  coordinate system is taken to be at the centre of the circular active area of the plane.

## 2.3 Stations and Spacepoints

The station reference surface is defined to coincide with the reference surface of the  $V$  doublet-layer. The station coordinate system is defined such that the  $x_s$  axis is coincident with the  $v$  coordinate (that is,  $\alpha$  for the  $V$  layer), the  $z_s$  axis is coincident with the  $z_p$  axis of the  $V$  layer and the  $y_s$  axis completes a right-handed  
85 coordinate system.

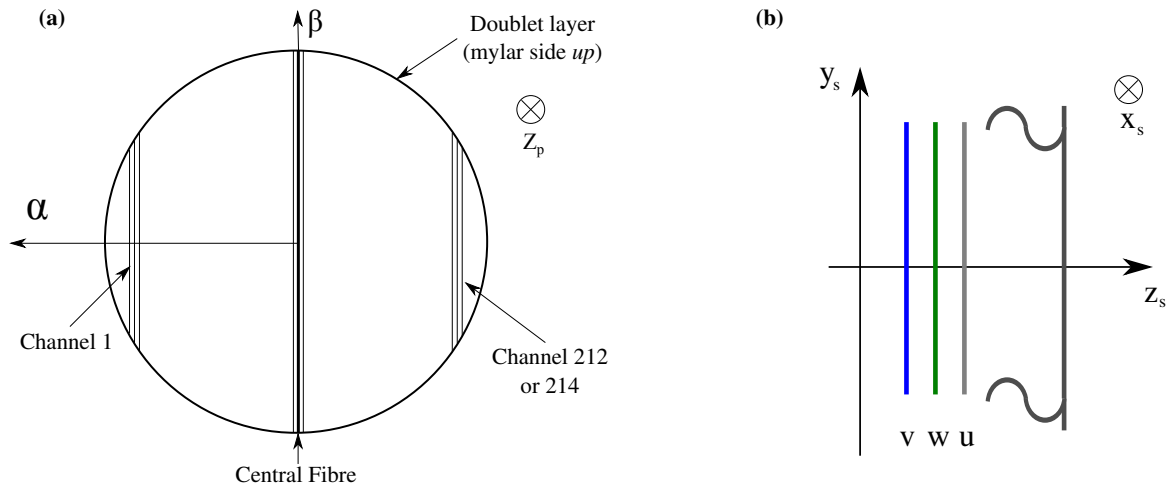
## 2.4 Trackers and Tracks

The tracker reference surface is defined to coincide with the reference surface of Station 1. The tracker coordinate system is defined such that the  $z_t$  axis coincides with the axis of cylindrical symmetry of the tracker as shown in figure 2. The tracker  $z_t$  coordinate increases from Station 1 to Station 5. The tracker  $y_t$  axis is defined  
90 to coincide with the  $y_s$  axis of Station 1 and the tracker  $x_t$  axis completes a right-handed coordinate system.

## 3 The MAUS Framework

The tracker software is part of the MICE software framework, known as MAUS (MICE Analysis User Software) [7]. MAUS is used to perform Monte Carlo simulation and both online and offline data reconstruction. It is built using a combination of C++ and Python, with C++ being used predominately in the code used for  
95 more processor intensive tasks (the “backend”) and Python being used more in the code presented to the user (the “frontend”). Simulation is supported by GEANT4 [8], and analysis with ROOT [9]. The input and output data formats can be either ROOT or JavaScript Object Notation (JSON) files (with ROOT being the standard). MAUS also reads in the custom binary format written by the MICE data acquisition system (DAQ).

MAUS is controlled by the user using a top level Python script, together with a configuration file. The  
100 structure at the top level is set out in a functional-coding manner, with different modules being loaded depending on the task at hand. The modules come in four types: Input; Output; Map; and Reduce. Input modules provide the initial data to MAUS, from a data file, or from the DAQ. Maps perform most of the simulation and analysis work and may be processed in parallel across multiple nodes. Reducers are used to display output, such as for online reconstruction plots, and are capable of accumulating data sent from maps over multiple spills, but must  
105 only be run in a single thread. Output modules provide data persistency by saving to a file in a standard format.



Fibre run to the station optical connectors towards the bottom of the figure

Figure 5: (a) The channel numbering within a plane, and the  $(\alpha, \beta, z_p)$  plane coordinate system (a right-handed system). (b) The fibre plane ordering with respect to the station body and the station coordinate frame (a right-handed system). In TKU the beam approaches from the right, in TKD from the left. Note that  $z_s$  is by definition equivalent to  $z_p$  of the  $V$  plane.

The tracker software is called using four maps and a reducer. The maps cover: digitisation of Monte Carlo data; digitisation of real DAQ data; the addition of noise to Monte Carlo data; and reconstruction. The reducer provides event plots and run information. The modules contain little code themselves but instead call backend C++ classes.

## 4 Data Structure

### 4.1 General MAUS, Monte Carlo and DAQ data structures

A simplified schematic of the tracker data structure, with the relevant entries from the more general MAUS data structure, is shown in figure 6. All the objects listed represent container classes for different parts of the simulation, raw data and reconstruction. The top level object is known as the spill, which contains the data associated with the burst of particles produced by one dip of the pion production target. Within the spill the data is split into three branches: real data from the DAQ; Monte Carlo data generated by simulation; and reconstruction data, which is formed from data in either the real or Monte Carlo branches.

The reconstruction code makes no direct reference to the Monte Carlo information, and has no way to distinguish real from simulated data, thus ensuring that they are treated equally. The real DAQ data is held in an object known as TrackerDAQ. This is then further split depending on where the raw data originated; if from the full MICE DAQ then it is stored in a VLSB object or, if the data originated in a cosmic-ray test DAQ, in a VLSB\_C object.

The Monte Carlo event holds data on scifi hits produced by tracks passing through sensitive volumes (the fibre planes) and any associated noise hits originating in those planes. The scifi hit is implemented as a class based on the generic Hit class template from which all the different MICE Monte Carlo detector hit classes are derived (see [7]). Other relevant data held in the Monte Carlo event, though not part of the tracker data structure, includes simulated track objects which hold the generated information on position, momentum and particle type. Such data is used to evaluate the reconstruction performance against the generated data (see



Figure 6: The tracker software data structure, and relevant MAUS data structure. The spill is the top level object below which data is split into real data, MC data and reconstruction sides. When an object owns the memory of a set of other objects, these are held as standard vectors of pointers. When an object contains cross links to another set of objects, without owning their memory, these are held as a ROOT TRefArray of pointers. SPR = Straight Pattern Recognition, HPR = Helical Pattern Recognition.

section 8).

## 4.2 Tracker reconstruction data structure

The reconstructed data for the tracker is held in the SciFiEvent class. This contains C++ standard library vectors of the following container classes that represent the higher level reconstructed tracker data:

- “SciFiDigits” represent the digitisation of a detector channel response to an incident track;
- “SciFiClusters” represent groups of neighbouring Digits arising from the same particle crossing multiple channels;
- “SciFiSpacepoints” group Clusters from adjacent detector planes to give a real space position in terms of  $(x, y, z)$ ;
- “SciFiStraightPRTracks” group together Spacepoints from different tracker stations when the originating track is straight (i.e. when the enclosing field is off).
- “SciFiHelicalPRTracks” group together Spacepoints from different tracker stations when the originating track is helical (i.e. when the enclosing field is on).
- “SciFiTracks” hold the final Kalman fit parameters of the particle track. SciFiTracks also contain SciFiTrackPoints, which hold the fit parameters at each detector plane, including the momentum and position of the track.

## 4.3 Cross links and the Monte Carlo - Reconstruction bridge

Each higher level object also contains cross links in the form of pointers back to the objects within the SciFiEvent which were used to create it; thus Clusters contain pointers to Digits, Spacepoints to Clusters, Pattern

Tracker 1 offsets in mm					
	Station 1	Station 2	Station 3	Station 4	Station 5
X	0.0	-0.5709	-1.2021	-0.5694	0.0
Y	0.0	-0.7375	-0.1657	-0.6040	0.0
Z	-1099.7578	-899.7932	-649.9302	-349.9298	0.0

Tracker 2 offsets in mm					
	Station 1	Station 2	Station 3	Station 4	Station 5
X	0.0	-0.4698	-0.6717	0.1722	0.0
Y	0.0	0.0052	-0.1759	-0.2912	0.0
Z	-1099.9026	-899.009	-650.0036	-350.0742	0.0

Table 1: Position of tracker stations from CMM measurements, positions taken with respect to reference surface.

Recognition Tracks to Spacepoints, and SciFiTracks to Pattern Recognition Tracks. In this manner all higher level objects can be traced back fully to the original Digits.

In the case of a Monte Carlo run the Digits themselves are linked via an ID number and lookup table back to the Monte Carlo hits used to produce them. The ID is defined as  $tsppcc$ , where  $t$  is the tracker number,  $s$  is the station number,  $p$  is the plane number, and  $c$  is the channel number. This structure means the reconstruction branch has no direct reference to the Monte Carlo data.

## 5 Geometry

The absolute position of each tracker station was determined by use of a coordinate measuring machine (CMM) at Imperial College London [6]. The measurements were made by supporting the trackers upon blocks on the CMM. The tracker was not fixed to the supports to avoid introducing extra stresses which might distort the frame. The position of the stations was then determined with respect to station 5. (see table 1).

Tracker station positions are stored in the MICE configuration database (CDB). The CDB is a bitemporal database, alterations are tracked by date and run number, ensuring the proper geometry is used in analysis of historic data. Configurations are stored in the CDB as a collection of XML files which are translated into the native MAUS format "MICE modules", at run-time. The MICE modules are text documents and contain all the information needed to simulate the various MICE systems and detectors. The rotation convention adopted in all the MAUS geometry is that of interpreting rotations as passive rotations of the coordinate axis, as opposed to active rotations of the geometry elements. This is done in order to stay consistent with GEANT4.

MAUS uses the same detector geometry descriptions for both Monte Carlo and real data and may be called on by the reconstruction as needed. The only differences between the Monte Carlo and the real geometries relate to non-active portions of the experiment and field mapping. In particular, only the Monte Carlo geometry contains the epoxy resin, which was used in securing the individual scintillating fibres to the tracker station body, and the mylar sheets to support each doublet-layer. The carbon fibre body of the trackers have not been included in either the real or Monte Carlo geometries as their effect on the beam is expected to be minimal. The active volume of each tracker is given by a cylinder of 150 mm radius, which is used to define the fiducial volume for the reconstruction.

Alignment of the individual tracking stations and the trackers themselves to the solenoid axis will be completed using data taken during commissioning.

## 6 Simulation

The simulation of the MICE trackers is designed as a module for the MAUS software framework. The simulation makes use of the GEANT4 standard physics libraries to describe a particle motion's through the scintillating fibre material and uses various statistical models in describing the effects of electronic noise. The trackers are simulated on a per fibre basis and layered into the fibre planes in the expected doublet layer as shown in figure 3.

The MAUS framework invokes a beamline module to generate a simulated beam, according to pre-defined user parameters. A particle incident upon a tracker fibre is stepped through, in accordance with the defined parameters. GEANT4 is invoked in each of these steps in determining the resulting momentum change of the particle and the magnitude of energy deposited into the fibre. These values are recorded individually, the current step used in determining where the next step is taken, and recorded before the next step is processed. After a defined number of particles have been generated and stepped through the experiment the results are collected into a MICE spill and sent to the tracker MC module for processing.

Each one of the incoming MC hits has a simple conversion factor applied which determines the raw number of photo electrons (NPE) generated. A single interaction with a scintillating fibre is simulated by many steps through the material and the figure for any one step is not limited to integer values. The raw NPE from every step through the fibre is summed and feed into the simulation of noise in the tracker electronics (see section 6.1).

The final result from this process, which includes the channel number, the final processed NPE, and timing information from GEANT4 are used to create a SciFiDigit. This final result is as described in section 4.1, and the output Digit from the MC is identical to that created from DAQ data. After all hits have been processed the data is handed back to MAUS to be processed by the tracker reconstruction modules.

### 6.1 Noise

The MC noise simulation consist of two modules, false signal due to thermally excited electrons within the VLPC cassettes and a smearing due to random noise in the tracker electronics. This is in addition to noise introduced by particle decays handled outside of the tracker MC by the GEANT4 simulation.

Simulation of the thermally excited electrons is performed before the smearing simulation. The dark count is an uncorrelated process that is selected to occur with a magnitude of 1.0 PE in 1.5% of a data taking window. Actual rate is determined by the setting of the voltage bias in the VLPC cassettes which as a direct effect on the final signal size. The process is described as a Poisson distribution. Studies are underway to understand this effect in each cassette.

The results from the GEANT4 physics simulation and the Poisson dark count simulation are combined and smeared to determine the final NPE signal. The signal from the GEANT4 simulation can take any value, however, it is unreasonable to expect anything other than an integer number of photons, as such this incoming signal is changed to its nearest integer value. The value is smeared as described by a Gaussian with a sigma derived from a study of carried out in May 2012 of a single station in beam.

The smeared result is then fed through a process that simulates the effects of the analog to digital converters (ADCs). This process serves to chop the information up into bins of  $2^8$  discreet values. The exact values of these bins is determined from the tracker calibrations and varies with the with the channel placement into the electronics. Overflows are equivalent to the maximum signal.



## 7 Reconstruction

The reconstruction process is illustrated in figure 7 for both real and simulated data.

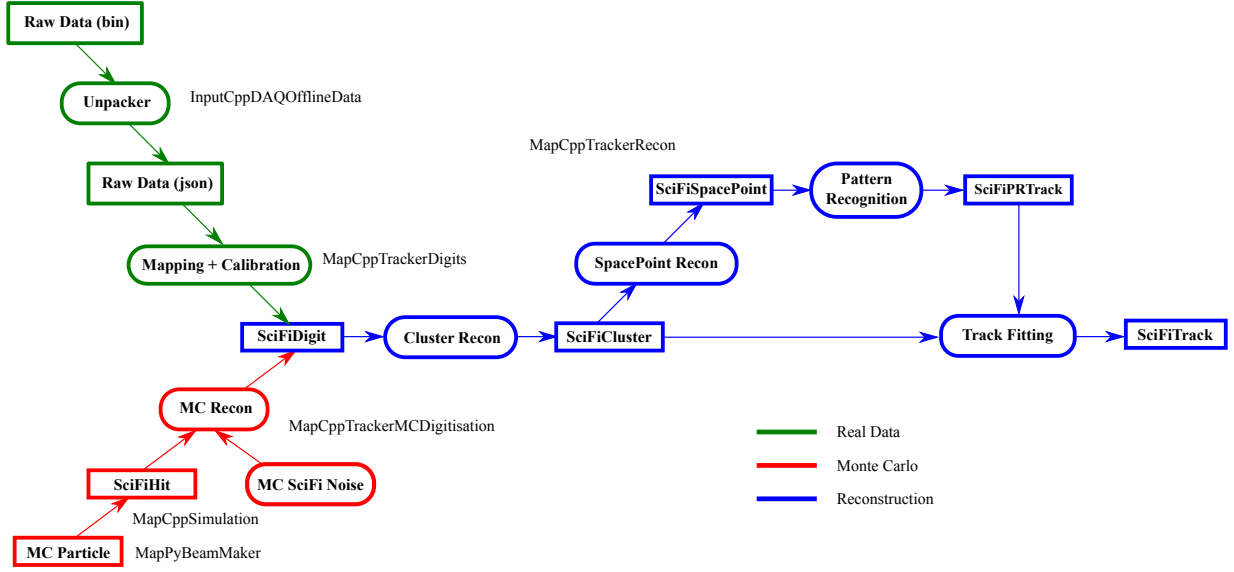


Figure 7: The reconstruction data flow. Data originates either from simulated or real data, the two branches meet after Digitisation, after which the reconstruction proceeds identically for both. The relevant MAUS modules for each step are indicated.

### 7.1 Digitization

For real data the electronic signals produced by the VLPCs are Digitised using analogue-to-Digital converters (ADCs). The DAQ system records the pulse height for each DAQ channel. Channel-by-channel calibration constants are used to convert the ADC value to a signal in units of photo-electrons (PE) and the VLPC channel number to tracker channel number. This information is then used to form a Digit. The analogous process for Monte Carlo data is described in section 6.

### 7.2 Clustering

A particle that traverses a plane will generate a hit in one or at most two adjacent channels. An isolated hit or hits in two adjacent channels form a Cluster.

The Clustering algorithm loops over every combination of pairs of Digits in a SciFiEvent and combines any that occur in neighbouring channels in the same plane. In the case of multi-Digit Cluster, the average channel value is used. The Cluster positioning is defined by the coordinates  $(\alpha, \beta)$  where  $\alpha$  and the direction of  $\beta$  have been defined in Section 2.2. In the case of two overlapping active channels the value for  $\beta$  is determined by solving:

$$\begin{pmatrix} \alpha_1 \\ \beta_1 \end{pmatrix} = R_1^{-1} R_2 \begin{pmatrix} \alpha_2 \\ \beta_2 \end{pmatrix} \quad (2)$$

where  $R_1, R_2$  are the rotation matrices that correspond to the orientation of the specified plane.

### 7.3 Spacepoint Reconstruction

For each station the constituent planes are searched for Clusters which can be used to define a Spacepoint. Spacepoints are defined by Clusters from all three planes (a triplet Spacepoint) or for any two out of the three planes (a doublet Spacepoint). From the Cluster coordinates,  $(\alpha, \beta)$ , the  $(x, y)$  coordinates of the Spacepoint are determined by rotating into tracker frame.

#### 7.3.1 Cluster selection

In order to determine which Clusters from each plane originate from the same track we follow Kuno's conjecture[6] which states that, for a given triplet Spacepoint, the sum of the channel numbers of each Cluster will be a constant. So if  $n^u$ ,  $n^v$  and  $n^w$  are the fibre numbers of the Clusters in  $u$ ,  $v$  and  $w$  and  $n_0^u$ ,  $n_0^v$  and  $n_0^w$  are the corresponding central channel numbers. Three Clusters form a space point if:

$$|(n^u + n^v + n^w) - (n_0^u + n_0^v + n_0^w)| < K. \quad (3)$$

where  $K$  is a constant, take by default as 3.0.

Once all triplet Spacepoints have been found, doublet Spacepoints are created from pairs of remaining Clusters.

### 7.4 Pattern Recognition

Pattern recognition is based on looping over different combinations of Spacepoints and performing a fit using a simple linear least squares technique. The algorithm treats helical and straight tracks separately, though much of the code is shared. Helical track finding is attempted first then, once all possible helical tracks have been found, any remaining unmatched Spacepoints in the SciFiEvent are passed to the straight line fitting routines.

#### 7.4.1 Helical Pattern Recognition

The helical pattern recognition is performed in cylindrical co-ordinates  $(r, \phi, z)$  where the turning angle  $\phi$  defined for  $0 \rightarrow \infty$  is distinguished from  $\phi'$  the reduced turning angle defined for  $0 \rightarrow 2\pi$ . For the helix  $s$  is the distance the particle travels measured along the helix. The helix is described by: the circle it describes in the transverse plane  $(x_{centre}, y_{centre}, radius)$ ;  $s_0$  the value of  $s$  where the helix crosses the reference plane; and  $t_s = ds/dz$ , which describes the tightness of the coiling.  $\phi_0$ , the angle of the track as it crosses the tracker reference plane, equivalent to  $s_0$ , is also used.

To find a track one Spacepoint is selected from each station and a circle is fitted in the  $(r, \phi')$  projection. If the  $\chi^2$  of this fit is sufficiently small (by default less than 15.0 multiplied by the number of degrees of freedom) then the value of  $\phi$  is used to generate  $s$  and a straight line fit is performed in the  $(z, s)$  plane, and if the  $\chi^2$  in this projection is also small (by default less than 4.0 multiplied by the number of degrees of freedom) the track is accepted.  $\phi$  itself is determined from  $\phi'$  by exploiting the different distances in  $z$  between successive tracker stations. The change in  $\phi$  between the hits in any two stations, divided by the distance between those stations, gives a constant which is the same for any pair of hits. This can then be used to infer the true values of  $\phi$ .

All possible combinations of five Spacepoints, one from each station are tested. Points can only be associated with one track. Then all combinations of any remaining Spacepoints are searched, this time requiring Spacepoints from four out of the five stations to form a helix. Tracks with momentum almost parallel to the solenoid axis (i.e. with low transverse momentum,  $p_T$ ) will not suffer an appreciable bend and will not be found by the

265 helix search and so any Spacepoints remaining after the helical tracks have been found are passed to the straight track finding algorithm.

## 7.4.2 Straight Line Pattern Recognition

270 Straight lines are fitted to the Spacepoints when there is no magnetic field and on any Spacepoints remaining after the helix fit is complete. The latter is to identify tracks with a small  $p_T$  which are not bent sufficiently in the magnetic field to form a recognisable helix (it has been observed from Monte Carlo studies that the efficiency of the helix finding algorithm begins to tail off for tracks with  $p_T < 10 \text{ MeV}/c$ ).

275 The fit is done in Cartesian coordinates and the track parameters are:  $(x_0, y_0, t_x, t_y)$  where  $t_x = dx/dz$  and  $t_y = dy/dz$ . Two Spacepoints are chosen in the outer chambers and a road is created between them. Any Spacepoints in the road are fitted, using Least Squares, in the  $(x, z)$  and  $(y, z)$  planes. The Spacepoints with the lowest  $\chi^2$  are chosen as long as their value is less than a predefined cut value (by default less than 15.0 multiplied by the number of degrees of freedom). As in the helical case, following the completion of the full 5 point track search, tracks with Spacepoints in 4 out of the 5 stations are searched for. For the straight case only, following the completion of the search for 4 point tracks, a search is also made for tracks with Spacepoints in only 3 out of the 5 stations.

## 280 7.5 Track Fit

The final track fit was implemented using a track-orientated Kalman filter[10, 11], which can be shown to be an optimal linear fitter, that takes into account all correlations and measurements, for a linear system. The Kalman Filter is an iterative algorithm that incrementally propagates an estimate of the current track state between measurement planes, using measurement information to “filter” the state, improving the estimate of the track state.

285 For the helical track fit, the system is only approximately linear, hence an extended Kalman filter was implemented which analytically propagates the track states between measurements, while the covariance matrices are propagated using a first-order linear approximation to the non-linear system.

290 Pattern recognition provides a set of Clusters that are associated with a track, which passed the selection criteria, and a parameterisation of that track based on a least squares fit to the points by a helix or a straight line as appropriate. The track parameters calculated from the least squares fit are used to provide the seed for the Kalman fit and the raw Cluster information is used as the measurement data. The flexibility of the Kalman algorithm permits the effects of individual planes (multiple coulomb scattering (MCS) and energy loss), in addition to the material effects of the Helium gas within the tracker, to be accounted for between each measurement point.

### 7.5.1 Kalman Filtering

The track is modelled as a discrete state space function of  $z$  (the direction of the beam), indicated by the subscript,  $k$ , where each tracker plane corresponds to a trackpoint and contains a measurement and a track state. Equation 4 describes how the true state space vector,  $\mathbf{x}_{k,t}$ , is assumed to propagate to a subsequent measurement plane. The matrix,  $\mathbf{F}_k$ , is the Kalman Propagator and describes the first order description of the propagation between measurement planes.  $\mathbf{w}_k$  represents some “process noise”, which may affect the system between the two measurement planes and is assumed to be gaussian distributed white noise.

$$\mathbf{x}_{k,t} = \mathbf{F}_{k-1} \mathbf{x}_{k-1,t} + \mathbf{w}_{k-1} \quad (4)$$

$$\exp(\mathbf{w}) = 0 \quad \text{and} \quad \text{cov}(\mathbf{w}) = \mathbf{Q}$$

The tracker measurements are interpreted in a different state space to the track, allowing measurements of any dimension to be used to filter the track. Equation 5 describes how the true track state is “measured” to be transformed into the measurement space. The matrix,  $\mathbf{H}_k$ , is the Kalman Measurement Matrix and describes, to first order, the transformation from track state space to the measurement state space.  $\varepsilon_k$  represents some “measurement noise” which may smear the measurement of the true state space, it is also assumed to be gaussian distributed.

$$\begin{aligned} \mathbf{m}_k &= \mathbf{H}_k \mathbf{x}_{k,t} + \varepsilon_k \\ \exp(\varepsilon) &= 0 \quad \text{and} \quad \text{cov}(\varepsilon) = \mathbf{V} \end{aligned} \tag{5}$$

For each measurement plane that contains a measurement, the current estimate for the track state vector is “filtered” using the measurement information. This is achieved using the residual between the estimate for the track state and the measurement data, in the measurement state space. Equation 6 describes how the predicted state vector,  $\mathbf{x}_k^{k-1}$  is filtered using the Kalman Gain Matrix,  $\mathbf{K}_k$ , to produce the filtered track estimate,  $\mathbf{x}_k$ . Equation 8 defines the Kalman Gain Matrix.

$$\mathbf{x}_k = \mathbf{x}_k^{k-1} + \mathbf{K}_k (\mathbf{m}_k - \mathbf{H}_k \mathbf{x}_k^{k-1}) \tag{6}$$

The predicted covariance matrix,  $\mathbf{C}_k^{k-1}$ , is filtered in a similar fashion to produce the filtered covariance matrix,  $\mathbf{C}_k^k$ , as described in equation 7:

$$\mathbf{C}_k = (\mathbf{I} - \mathbf{K}_k \mathbf{H}_k) \mathbf{C}_k^{k-1} \tag{7}$$

The Kalman Gain matrix is calculated by:

$$\mathbf{K}_k = \mathbf{C}_k^{k-1} \mathbf{H}_k^T (\mathbf{V}_k + \mathbf{H}_k \mathbf{C}_k^{k-1} \mathbf{H}_k^T)^{-1} \tag{8}$$

The sequence of prediction and filtering is repeated for all the measurement planes, starting from station 5, plane 2, where the predicted state vector and covariance matrix is determined from the pattern recognition fit parameters, to station 1, plane 0, the reference plane. Once the reference plane has been reached, the state vector will have been sequentially filtered using all the measurements in turn to create the optimal estimate of the track state at that plane. The fit can then be smoothed, whereby the optimal state vector is propagated in reverse down the length of the track, such that all the subsequent measurements can be used to re-adjust previous state vector estimates. This is described in [10]

### 7.5.2 The MAUS Kalman Filter Implementation

In order to implement a flexible re-usable Kalman Filter, the core algorithm was implemented without any dependencies on phase space dimensions or physical effects. Due to this only the system specific functionality need be provided for a complete implementation. The principal components of the implementation are: propagation routines for both helical and straight tracks; a measurement routine that correctly transforms the track state space into the measurement state space; and approximations for the process and measurement noise.

The measurements correspond to individual Clusters, hence the parameter  $\alpha$  (see section 2.2) forms a one-dimensional measurement state. The measurement noise corresponds to the statistical spread of measurements within a single channel in the tracker readout. If the channel is modelled as a top-hat function, the variance of the function is calculated as  $w^2/12$ , where  $w$  corresponds to the width of the channel. Therefore the measurement noise was assumed to be  $w/\sqrt{12}$  for all Clusters.

The process noise was implmented as a combination of MCS and energy straggling. The mean energy loss was is calculated using the Bethe-Bloch equation and applied during the propagation stage. The noise term

itself is calculated per increment, as an RMS scattering angle using an implementation of the Highland formula (equation 9), in a fashion almost identicle to the GEANT4 implementation:

$$\theta_{RMS} = \frac{13.6\text{MeV}/c}{\beta c p} z \frac{x}{X_0} \left( 1 + 0.038 \ln\left(\frac{x}{X_0}\right) \right) \quad (9)$$

where  $\theta_{RMS}$  is the RMS scattering angle through a finite length of material,  $\beta c$ ,  $p$  and  $z$  are the velocity, momentum and charge of the particle in question, and  $x/X_0$  represents the total path length through the material per radiation length. Although the RMS scattering angle does not form a gaussian distribution, the first order approximation is believed to be sufficient.

## 8 Performance

A high statistics Monte Carlo simulation was performed in order to estimate the reconstruction efficiency and resolution of the implemented track-finding and track-fitting algorithms. It was necessarily Monte Carlo based in order to compare the reconstructed events to the simulated truth, thereby highlighting any inefficiencies and inaccuracies within the algorithms, without any additional noise or biases.

The fitted transverse positions,  $(x, y)$ , and momenta,  $(p_x, p_y, p_z)$ , were compared against the the Monte Carlo truth on an event-by-event basis. The reconstructed events were not subject to any cuts or additional requirements over those of real data reconstruction. The Monte Carlo truth data was determined from the simulated track information, which was stored at every tracker plane to permit a direct comparison to the reconstructed data. All data sets were compared at the tracker reference surface, the designated measurement location with the MICE cooling channel.

An artificial beam was generated with uniform distributions in both the longitudinal and transverse momenta. This was to ensure that the results were not biased by the incoming beam distribution, and that the full reconstructable phase space was probed with equal statistics.

### 8.1 Track Finding Efficiency

For every simulated event, the number of expected tracks was calculated from the Monte Carlo truth. If the simulated track crossed enough tracker planes to create a sufficient number of spacepoints (3 for straight tracks and 4 for helical tracks), a reconstructed track was expected. The reconstructed tracks were then compared for each tracker and compared to the expected track parameters. The efficiency of track finding as a function of the true longitudinal and transverse momenta is shown in figure 8.

Once the the Monte Carlo tracks have been identified, the expected number of trackpoints can be calculated by examining the number of tracker planes that the simulated track crossed. Comparing the number of trackpoints in each reconstructed track to the expected number for each simulated track permits the efficiency of finding the correct number of trackpoints to be calculated. Figure 9 shows the trackpoint finding efficiency as a function of longitudinal and transverse momenta.

### 8.2 Reconstruction Resolution

Position residuals are shown in figures 10 and 11, and the momentum residuals in figures 12 and 13. The position reconstruction can be seen to agree with the Monte Carlo truth to high precision in both the upstream and downstream trackers. The momentum residuals currently display some systematic effect which is due to a known issue with the energy loss determination and is currently under study.

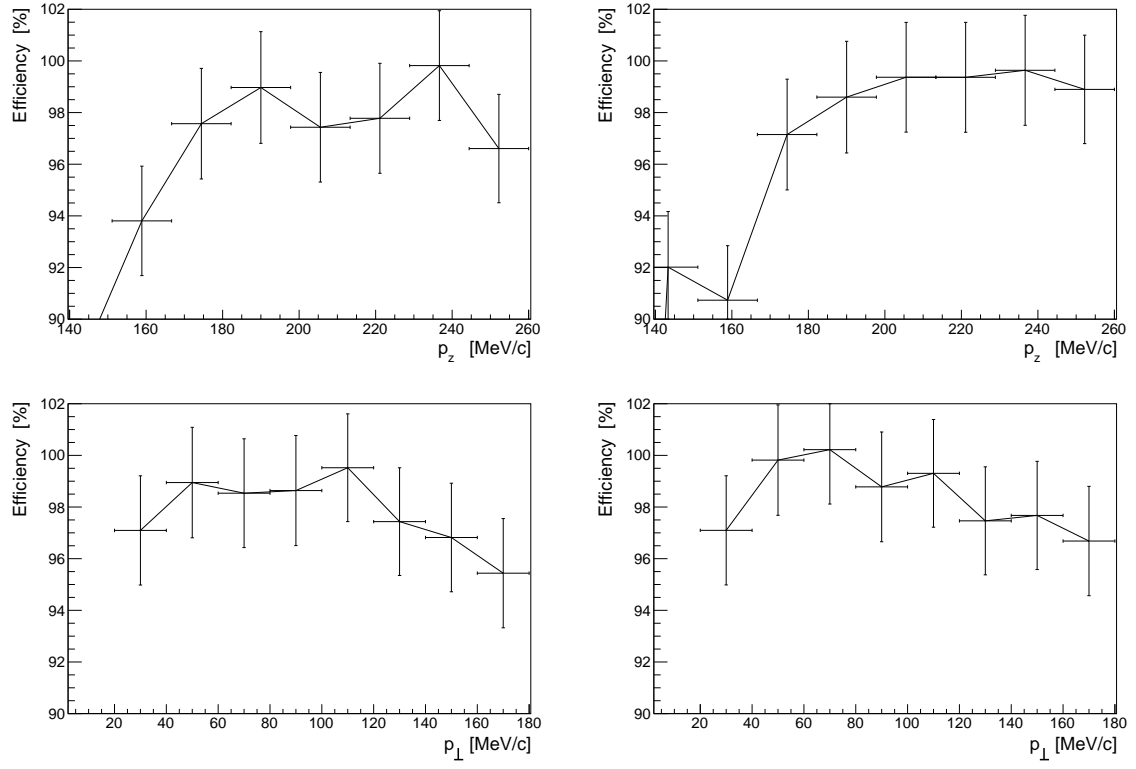


Figure 8: The efficiency of reconstructing tracks in the upstream (left) and downstream (right) trackers as a function of the simulated longitudinal (top) and transverse (bottom) momentum.

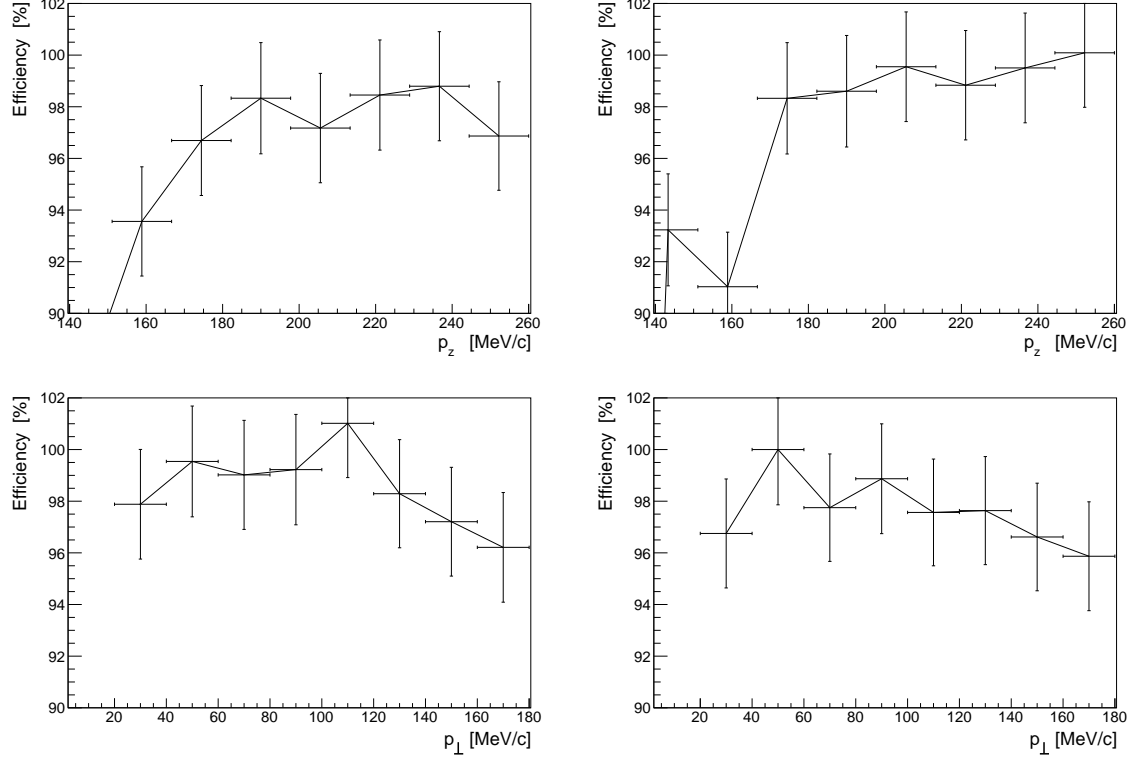


Figure 9: The efficiency of reconstructing trackpoints in the upstream (left) and downstream (right) trackers as a function of the simulated transverse momentum.

In order to produce these plots, a requirement that there was a cluster within the reference plane was applied.  
350 Due to the effects of Multiple Coulomb Scattering, on rare occasions a single hard scatter can cause pattern recognition to miss a single spacepoint at the reference plane, hence creating a tail that will adversely affect the distributions. As we are concerned with the resolution following a successful pattern recognition stage, these events were removed.

The position residuals are consistent with the expected measurement resolutions for a combined fit and the  
355 absolute spread is very close to the width of a channel (1.497mm). The transverse momentum resolution is consistent across the range of the sensitive phase space at  $\sim 1$  MeV/c in both trackers. The longitudinal momentum, an intrinsically more difficult measurement for the tracker, still retains an acceptable spread of  $\sim 3$  MeV/c in both trackers. There is however a systematic offset present in the distributions, 1.5 MeV/c in the upstream tracker, and 3.5 MeV/c in the downstream, and the distributions have more pronounced tails than in  
360 the transverse cases. These offsets require further investigation.

Trends in transverse and longitudinal momentum resolution as a function of transverse momentum are shown in figures 14 and 15. A consistently uniform distribution is found in the transverse momentum as expected, with the predominant issue found in the longitudinal reconstruction of low- $P_t$  tracks. This effect, when coupled with variations in efficiency will yield some systematic concerns in the reconstruction of statistical quantities such  
365 as emittance. Studies of these systematic biases are currently underway.

## 9 Conclusion

The performance for the final Kalman filter based track fit has been evaluated by comparing Monte Carlo truth with reconstructed data, for the key tracker measurements of  $x$ ,  $y$ ,  $p_\perp$  and  $p_z$ . The observed performance in the transverse position and momentum measurements is excellent, for both the upstream and downstream trackers.  
370 A systematic offset in  $p_z$  requires further investigation, though the resolution remains acceptable.

Future Monte Carlo studies will evaluate the performance of the MICE emittance measurement and how the resolutions of the trackers could bias the measurements.

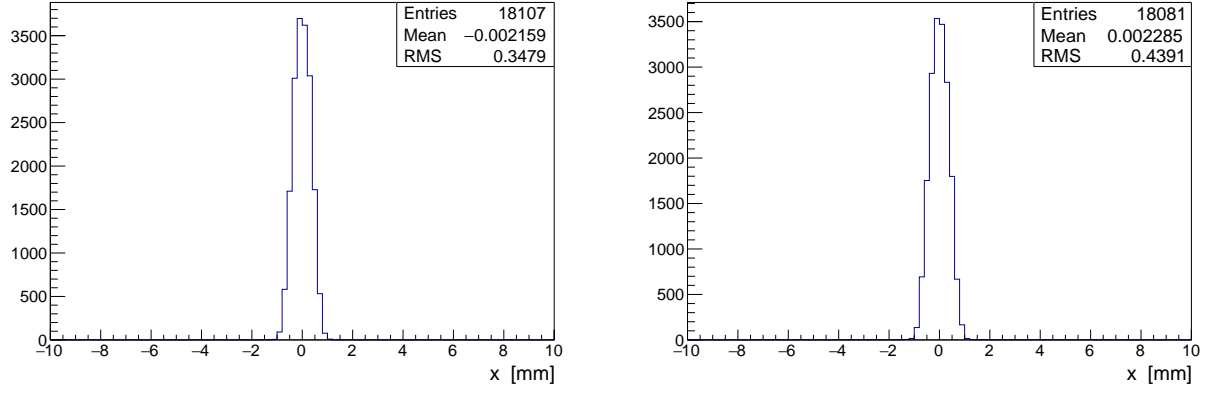


Figure 10: The  $x$  residuals of the upstream (left) and downstream (right) trackers for a 6 mm 4D emittance, and 200 MeV/c momentum beam.

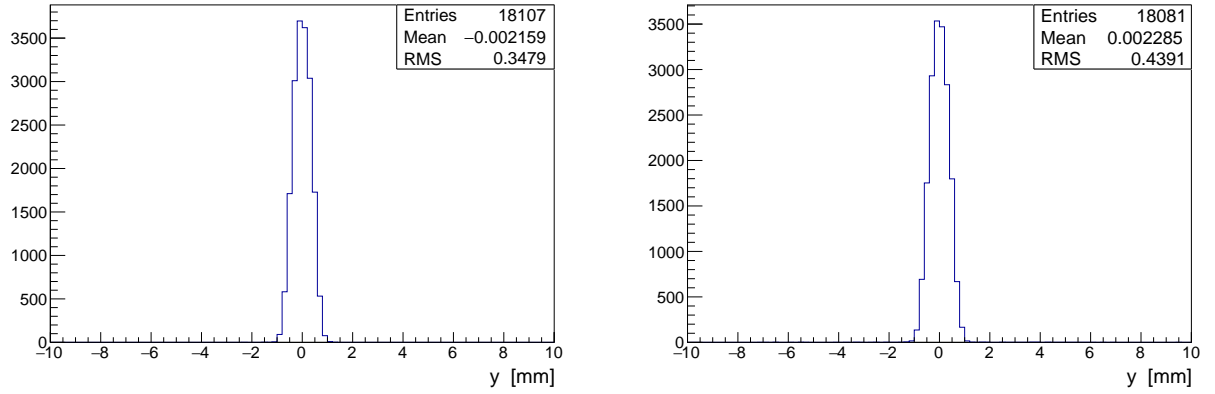


Figure 11: The  $y$  residuals of the upstream (left) and downstream (right) trackers for a 6 mm 4D emittance, and 200 MeV/c momentum beam.

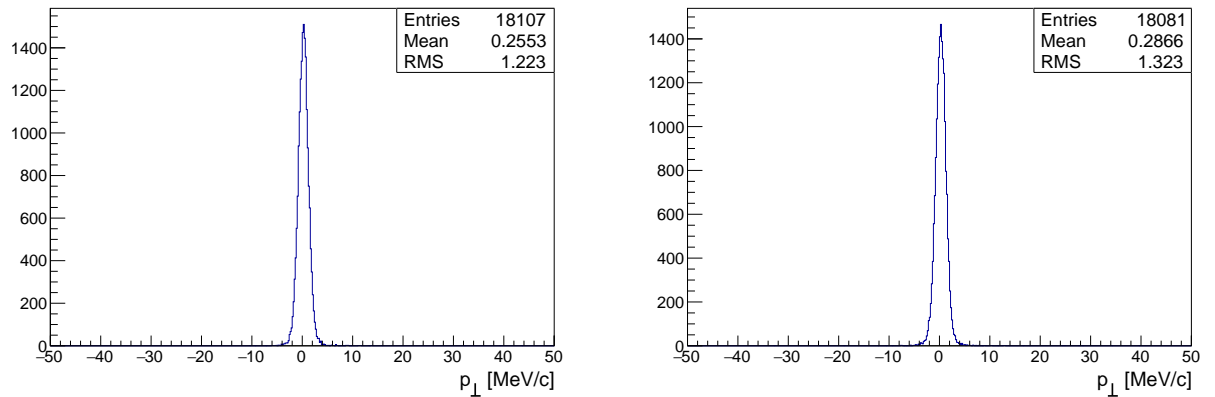


Figure 12: The  $p_{\perp}$  residuals of the upstream (left) and downstream (right).



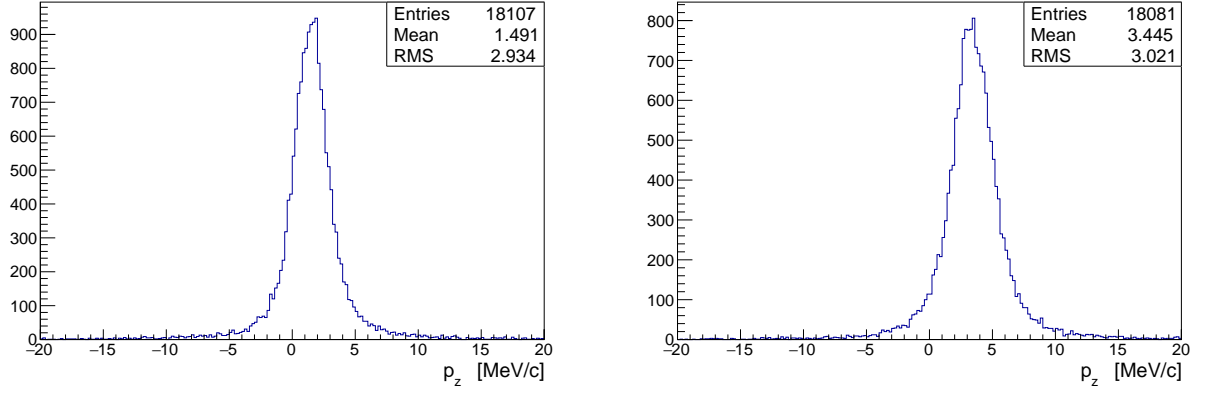


Figure 13: The  $p_z$  residuals of the upstream (left) and downstream (right) trackers for a 6 mm 4D emittance, and 200 MeV/c momentum beam.

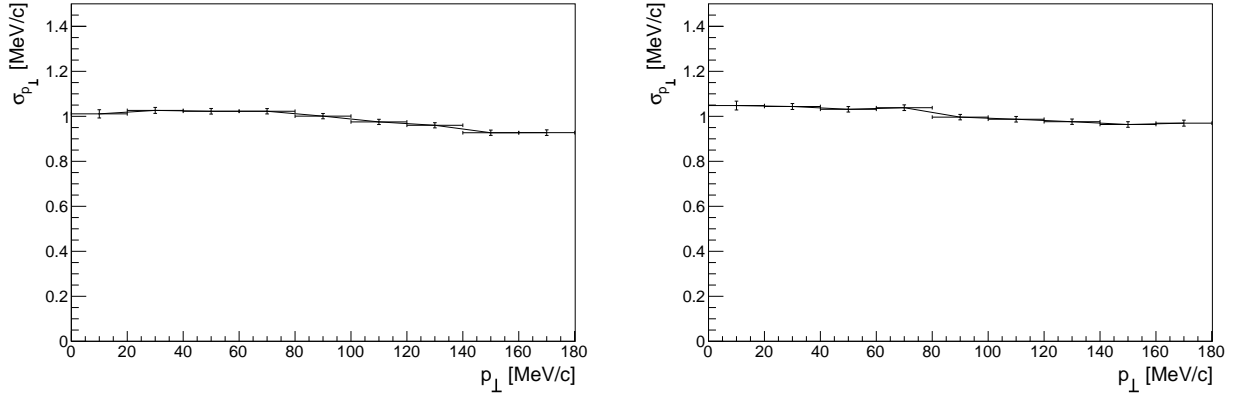


Figure 14: The  $p_{\perp}$  resolution vs the  $p_{\perp}$  of the upstream (left) and downstream (right).

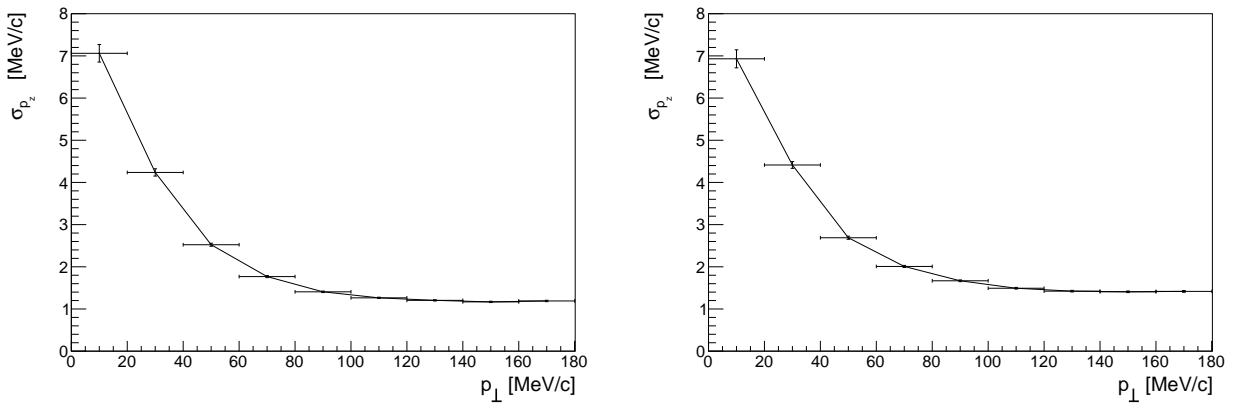


Figure 15: The  $p_z$  resolution vs the  $p_{\perp}$  of the upstream (left) and downstream (right).

## References

- [1] International Scoping Study Physics Working Group, “Physics at a future Neutrino Factory and Superbeam facility,” *Rep. Prog. Phys.* **72** (2009) 106201. arXiv:hep-ph/0710.4947v2.
- [2] S. Geer, “Muon Colliders and Neutrino Factories,” *Annual Review of Nuclear and Particle Science* **59** (2009) 345 – 367.
- [3] A. Skrinsky and V. Parkhomchuk, “Cooling methods for beams of charged particles,” *Sov. J. Part. Nucl.* **12** (1981) 223 – 247.
- [4] D. Neuffer, “Principles and applications of muon cooling,” *Part. Accel.* **14** (1983) 75.
- [5] M. Bogomilov *et al.*, “The MICE Muon Beam on ISIS and the beam-line instrumentation of the Muon Ionization Cooling Experiment,” *JINST* **7** (2012) P05009, arXiv:1203.4089.
- [6] M. Ellis, P. Hobson, P. Kyberd, J. Nebrensky, A. Bross, *et al.*, “The Design, construction and performance of the MICE scintillating fibre trackers,” *Nucl.Instrum.Meth.* **A659** (2011) 136–153, arXiv:1005.3491 [physics.ins-det].
- [7] D. Rajaram, “MAUS: The MICE Analysis and User Software.”. Currently in production.
- [8] S. A. et al., “Geant4 - a simulation toolkit,” *Nucl. Inst. Meth. A* **506** (2003) 250.
- [9] R. Brun and F. Rademakers, “Root - an object oriented data analysis framework,” *Nucl. Inst. Meth. A* **389** (1997) 81–86. <http://root.cern.ch/>.
- [10] R. Fruhwirth, “Application of kalman filtering to track and vertex fitting,” *Nucl. Instrum. Methods Phys. Res. A* **262** no. HEPHY-PUB-503, (Jun, 1987) 444. 19 p.
- [11] P. Billoir, “Track fitting with multiple scattering: A new method,” *Nucl. Instrum. Methods* **225** no. 2, (1984) 352 – 366.